

Low-viscosity oligoether esters (OEEs) as high-efficiency lubricating oils: Insight on their structure–lubricity relationship

Hanwen WANG^{1,2}, Ying WANG¹, Ping WEN¹, Lin MA¹, Mingjin FAN^{1,*}, Rui DONG^{1,*}, Chunhua ZHANG^{2,*}

¹ Shaanxi Key Laboratory of Phytochemistry, College of Chemistry & Chemical Engineering, Baoji University of Arts and Sciences, Baoji 721013, China

² Key Laboratory of Shaanxi Province for Development and Application of New Transportation Energy, Chang'an University, Xi'an 710064, China

Received: 12 January 2023 / Revised: 16 February 2023 / Accepted: 21 March 2023

© The author(s) 2023.

Abstract: Development of energy-efficient lubricants is a way to reduce energy consumption for transportation, with the tendency to design molecules that are beneficial in reducing the viscosity of synthetic oils. Oligoether esters (OEEs), as a low-viscosity ester base oil, have characteristics such as simple synthesis and excellent lubrication effect; however, the application of OEEs in tribology field has rarely been investigated. The objective of the present study is to investigate the effect of structure on the lubricating performance of OEEs and to develop a predictive model for OEEs based on quantitative structure–property relationship (QSPR) through a combination of experiment and statistical modeling. Results showed that glycol chains contribute positively to lubrication with the ether functional groups increasing the sites of adsorption. Compared to branched-chain OEEs, straight-chain OEEs exhibited reduced wear, which was mainly due to the thicker adsorption film formed by the straight-chain structure. Furthermore, carbon films were detected on lightly worn surfaces, indicating that OEEs underwent oxidation during the friction process. Based on the results of principal component analysis (PCA) and partial least squares (PLS), it could be found that the predictive models of viscosity–temperature performance, thermal stability performance, coefficient of friction (COF), and wear volume (WV) performed well and robustly. Among them, COF and WV can be best predicted with an R^2 of about 0.90.

Keywords: oligoether esters (OEEs); low-viscosity ester; friction; wear; quantitative structure–property relationship (QSPR)

1 Introduction

Energy scarcity and increasingly stringent emission regulations have led researchers in the internal combustion engine industry to pay attention to green lubricants. According to statistics, new tribological technologies (such as advanced friction materials and low-viscosity lubricants) can triple fuel economy by reducing friction losses in internal combustion engines [1]. In the operation of internal combustion engines, evaporation of light fractions, self-oxidation, and

particle contamination from fuel combustion can lead to an increase in lubricant viscosity [2], causing high energy consumption to overcome flow resistance. To address this problem, the service life of lubricants is improved by lubricant additives such as dispersant, detergent, antioxidant, and friction modifier. However, although the lubricity performance of fully formulated lubricants is mainly determined by additives, one of the most fundamental and effective ways to reduce viscosity is to develop low-viscosity base oils [3, 4].

Benefited from the excellent lubricity performance,

* Corresponding authors: Mingjin FAN, E-mail: fanmingjin@bjwxy.edu.cn; Rui DONG, E-mail: dongruibj@163.com; Chunhua ZHANG, E-mail: zchzz@126.com

low temperature flow properties, thermal stability, and biodegradability, synthetic esters are widely used in aerospace [5], automotive [3], and other applications [6]. The most characteristic feature of synthetic esters is the presence of one or more ester bonds ($-\text{COOR}$) in their molecule, which contributes to the high polarity of the molecules. Polarity is positively correlated with the adsorption of molecules at the interface and the stability of the lubricating film. Polyether, as a representative synthetic lubrication material [7], the presence of ether bonds ($-\text{COC}$) can confer the molecule flexibility [8, 9], which largely related to its viscosity. By introducing ester groups while retaining the ether bond [10], the synthesized oligoether esters (OEEs) show remarkable physical and mechanical properties and readily biodegradable [11]. However, their application to lubricants and tribological properties has rarely been reported, besides, the quantitative structure–property relationship (QSPR) is also unclear.

Obviously, as the main components of OEEs, alkyl side chains and glycol chains are closely related to their physicochemical and tribological properties. Previous research has found that molecular weight (MW) [12], chain length [13, 14], and glycol number [15] can affect the thermal stability, physicochemical properties, and mechanical behavior of OEEs. Raof et al. [16] revealed that carbon chain length and branching had a positive effect on the oxidative stability of ester oils. Zhang et al. [17] found that molecular structures with linear-shapes have significantly reduced friction relative to molecules with bulky side chains. Recently, Airey et al. [18] revealed that the increase in the number of ester groups and the length of carbon chains could reduce friction by increasing the molecular packing efficiency on the friction surface. Furthermore, studies in recent years have found a correlation between the adsorbed mass at the lubricant–solid interface and the friction properties, which was inextricably linked to the structure of the ester functional groups as well as other polar functional groups in the molecules [19–21]. However, the influence of molecular structure on properties involves hydrogen bonding, atomic number, functional groups, electrostatic forces, branched chain types, intermolecular interactions, and so on, leading to the difficulty for obtaining systematic and

critical conclusions. And the previous studies focusing on these properties were all based on empirical or semi-empirical methods. Therefore, it is urgent to develop a more comprehensive modeling approach to explore the relationship between structure and property of OEEs. QSPR is an indirect and multidimensional method for analyzing the structure–property relationship of lubricants [6, 22]. Specifically, the massive 1D, 2D, and 3D molecular descriptors including the information on molecular theory, molecular composition, physicochemical properties, and molecular shape, are calculated by optimizing the molecular structure. Before modeling, molecular descriptors are necessarily screened to avoid overfitting with much information. The methods for modeling are diverse, such as stepwise regression [23], genetic algorithm (GA) [24], principal component analysis (PCA) [25], etc. In modeling, molecular descriptors are used as input variables, and lubricant properties, such as pour point (PP), coefficient of friction (COF), and wear volume (WV), etc., are used as output variables. Wan et al. [26] applied least squares support vector regression to model the correlation among molecular descriptors and anti-wear properties, and found that an increase in the longest fatty chain, relative molecular mass, and van der Waals volume was beneficial for the performance. Nasab et al. [27] developed a viscosity index (VI) and PP predictive model using partial least squares (PLS) and GA based on laboratory data of 41 ester lubricants and highlighted the 3D geometry, molecular connectivity, and spatial autocorrelation of ester oils.

OEEs can be prepared through esterification reactions between oligomers such as diethylene glycol, triethylene glycol, and carboxylic acids with simple synthesis methods [28]. Previous studies have focused on the effect of molecular structure on the tribological properties of conventional synthetic ester lubricants [16, 19, 29, 30]. Accordingly, the mechanism of the frictional effect of OEEs introduced with multiple ether functional groups has not been reported. The objective of present work is to investigate the effectiveness of molecular structure on the performance of OEEs, including physicochemical and tribological properties, and also to develop a model for predicting the performance of OEEs based on the QSPR method, which can be accurately applied to the estimation of

average COF and WV. Specifically, firstly, the effects of alkyl side chain length, glycol chain length, and branching on the performance of OEEs were explored separately. Then, the worn surface was analyzed using scanning electron microscopy (SEM), and wettability and adsorption properties of the OEEs were tested using a contact angle (CA) meter and a Q-Sense quartz crystal microbalance with dissipation (QCM-D), respectively. The mechanism behind the friction effect of OEEs was investigated by Raman spectroscopy and X-ray photoelectron spectroscopy (XPS). Finally, to further facilitate the development of OEEs lubricants, predictive models were developed using 13 molecular descriptors.

2 Materials and experimental

2.1 Materials

P-toluenesulfonic acid (98%) was provided by Energy Chemicals. Diethylene glycol (99%), diglycolic acid (99%), triethylene glycol (99%), tetraethylene glycol (99.5%), hexaethylene glycol (99.5%), butyric acid (99%), hexanoic acid (99%), octanoic acid (99%), dodecanoic acid (99%), and 2-ethylhexanoic acid (98%) were purchased from Aladdin Amethyst Chemical.

2.2 Synthesis and structural characterization

The abbreviation, raw materials, and preparing method details of the synthesized OEEs are stated in the Electronic Supplementary Material (ESM). The molecular structures of the OEEs were examined using Agilent 400 MHz nuclear magnetic resonance (NMR) based on proton NMR technique (^1H NMR, 400 MHz) and carbon NMR technique (^{13}C NMR, 100 MHz) by using CDCl_3 as solvent and TMS as internal standard. In addition, the presence of functional groups and chemical bonds was analyzed using Fourier transform infrared spectroscopy (FT-IR, Perkin Elmer Singapore).

2.3 Physicochemical properties

Kinematic viscosity (KV) differences between various OEEs lubricants with similar structures at 40 °C and 100 °C were quantified using a Stabinger viscometer (SVM 3000, Anton Paar) according to ASTM D7042-

2012 standard, after which their VI was automatically calculated. The flash point (FP) was recorded using a Stanhope-Seta flash point tester (82000-0, UK) according to ASTM D3828-09. PP was determined using an automatic pour point tester (DR4-22 L) manufactured by Lawler according to ASTM D97-09. The oxidation induction time (OIT) of the samples was recorded on a ROB tester (Stanhope-Seta 15,200 5, UK) according to ASTM D2272 2014. Thermal stability was evaluated using Netzsch's simultaneous thermal analysis system (DSC/DTA-TG, STA 449 F3).

2.4 Tribological test and mechanism characterization

An oscillating friction and wear tester (SRV-V Optimol Instruments, Germany), was chosen to perform tribological tests under reciprocating conditions. The friction couples consist of a ball (10 mm diameter, AISI 52100 steel) and a disc (24 mm diameter, AISI 52100 steel). Reciprocating motion is realized by a horizontal oscillating rod driving the lower disc at a fixed frequency, thus generating reliable tribological data. In friction test, temperature, frequency, and amplitude were kept at 25 °C, 25 Hz, and 1 mm, respectively. The normal load was set to 100 N, which corresponded to a maximum contact pressure of 2.15 GPa. Each sample was recorded for 1,800 s under the same operating conditions. In addition, all steel discs were polished with 400 Cw, 800 Cw, and 1,500 Cw SiC sandpaper before tribological test, respectively, followed by cleaning with ethanol. A non-contact surface profiler (BRUKER-NPFLEX) was used to measure the WV of the lower discs after friction and the wear rate was calculated. The microscopic morphology of the worn area was observed by a field emission scanning electron microscope (FE-SEM, Quanta FEG 250, USA). Wettability of lubricants can be quantified in terms of CA (Attension, Biolin Scientific AB, Sweden). The mass of the adsorbed film were measured with a Q-Sense quartz crystal microbalance with dissipation (QCM-D, Sweden Biolin Scientific AB). After SEM analysis, grinding pits for lower discs were checked by Raman spectroscopy (Renishaw inVia Raman, Britain) and X-ray photoelectron spectroscopy (PHI 5000, Japan). Each sample was tested three times and the mean and standard error were reported. Note

that detailed instructions for the calculation of the maximum contact pressure and wear rate can be found in Ref. [31].

2.5 Descriptors and modeling approaches

In the present work, we computed molecular descriptors using the PaDEL-Descriptor software, obtaining a total of 1,875 descriptors. Special attention was paid to the fact that all structures were entered in advance into the SYBYL software and their lowest energy 3D conformations were generated using the standard Tripos method. A detailed description of all the data, including 1,444 2D and 431 3D molecular descriptors for each category, can be found in Ref. [32].

The molecular descriptors, which can efficiently identify the isomers, have to be considered as the subject. Descriptors with standard deviations less than 0.0005, descriptors with pairwise correlations ≥ 0.95 , and descriptors with missing values were removed before making the selection of key descriptors. OEEs were divided into two groups according to whether the alkyl side chains were straight or branched, and the discriminative ability of different descriptors for spatially grouped data was weighed. Thirteen 3D molecular descriptors were finally selected after verifying that 1D and 2D molecular descriptors could not discriminate between structurally similar OEEs. The names and definitions are given in the Table S2 in the ESM.

2.6 Statistical analysis

Pearson correlation was performed in Minitab 19.0 (State College, PA) to investigate the correlation between the average COF and WV. The correlation coefficient (R) evaluated the strength of the correlation ($R = 1$, indicating a perfectly positive correlation between the two variables; $R = -1$, indicating a perfectly negative correlation between the two variables; $R = 0$, indicating no correlation).

PCA was performed in SPSS 26.0 (IBM Corp., Ltd., New York) to filter and downscale the molecular descriptors.

PLS was performed in Minitab 19.0 (State College, PA), and the optimal principal component score was determined.

The root mean square error (RMSE) as well as the coefficient of determination (R^2) were used as evaluation indicators to verify the validity of the model. RMSE and R^2 were calculated as Eqs. (1) and (2):

$$\text{RMSE} = \sqrt{\frac{1}{N} \sum_1^N (Y_{\text{Exp}} - Y_{\text{Pre}})^2} \quad (1)$$

$$R^2 = 1 - \frac{\sum_1^N (Y_{\text{Exp}} - Y_{\text{Pre}})^2}{\sum_1^N (Y_{\text{Exp}} - \bar{Y}_{\text{Exp}})^2} \quad (2)$$

where Y_{Exp} is the measured value and Y_{Pre} is the calculated value.

3 Results and discussion

3.1 Characterization

Three series of variable structures were designed: (1) length of alkyl chain, (2) length of glycol chain, and (3) branched alkyl chain, as shown in Figs. 1(a1), 1(a2), and 1(a3). 4g-2cy represents the first series of OEEs (Fig. 1(a1)). 4 is the number of glycols in the middle of the molecule, 2 is the alkyl chain at both ends, and y is the number of carbons in the alkyl chain. xg-2c8 and xg-2ci8 represent the 2nd and 3rd series of OEEs, respectively, and i stands for branched isomerism of straight-chain alkyl chains. The structure and purity of OEEs were confirmed with ^1H NMR and ^{13}C NMR, and detailed information can be seen in the ESM. Figures 1(b1)–1(b3) shows the FTIR spectra of the functional groups and the characteristic stretch features of synthetic lubricants. The peak rise at $1,734\text{ cm}^{-1}$ represents high intensity stretching band C=O. And the main absorption band in $2,924\text{--}2,859\text{ cm}^{-1}$ indicates Sp^3 C–H stretching vibration, as well as the absorption band of $1,466\text{ cm}^{-1}$ is the corresponding Sp^3 C–H bending vibration. Expectedly, the absorption band appeared in $1,215\text{--}1,034\text{ cm}^{-1}$, which is related to the stretching vibration of C–O groups. In addition, the prominent peaks of C–O bond at $1,106$ and $1,174\text{ cm}^{-1}$ are observed. Due to the highly structural symmetry, the peak at $1,106\text{ cm}^{-1}$ and $1,174\text{ cm}^{-1}$ are associated with ether and ester functional groups due to a high degree of structural symmetry [19, 33].

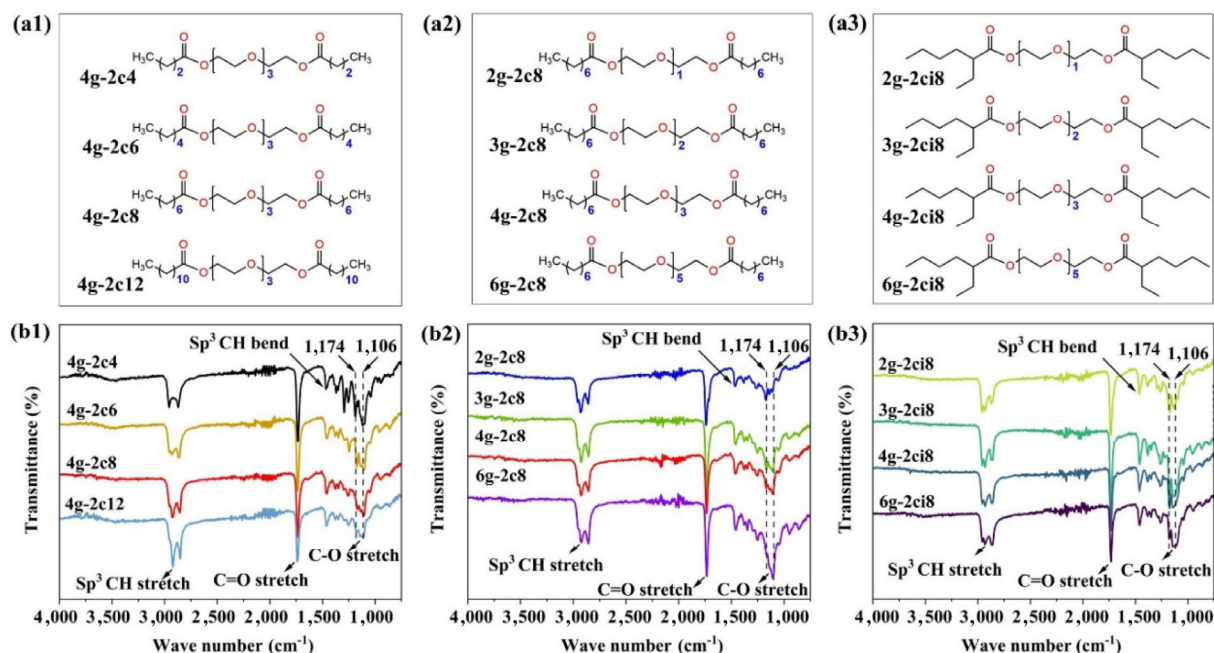


Fig. 1 Molecular structure of lubricants: (a1) 4g-2cy series; (a2) xg-2c8 series; (a3) xg-2ci8 series. FTIR spectra of lubricant: (b1) 4g-2cy series; (b2) xg-2c8 series; (b3) xg-2ci8 series.

3.2 Physicochemical property

To further demonstrate the low viscosity properties of OEEs, we compared them with commercially available synthetic esters. For instance, compared with diisooctyl sebacate (MW: 426.68) [19], 4g-2ci8 (MW: 446.32) is similar to its structure, however, KV at 40 °C and 100 °C is reduced by 11.43% and 13.80%, respectively. From Figs. 2(a) and 2(b), KV of all OEEs except 4g-2c12 (MW: 558) is below 16 mm²/s at 40 °C and below 4 mm²/s at 100 °C. In addition, KV shows linear increase correlation approximately with increasing MW. Here, KV of straight-chain OEEs with the same MW is higher than that of branched-chain OEEs. And, the decrease in KV is related to the introduction of the ether bond, which causes the molecules to undergo bending agglomeration and generates more free volume [34, 35]. Furthermore, straight alkyl chains have strong molecular rigidity and are not easily deformed, whereas branched chains are easily deformed and have better mobility [36]. VI reflects the degree of KV variation of the lubricant with temperature, the larger VI, the larger temperature range over which the lubricant can provide protection. Figure 2(c) presents VI of 4g-2cy, xg-2c8, and xg-2ci8, respectively. As shown, significant difference is observed

between the straight-chain and branched-chain OEEs. It basically confirms that, indeed, the intermolecular forces between the branched-chain OEEs decrease more under the condition of increasing temperature [37, 38]. In other words, straight-chain molecules have a stronger ability to resist the reduction of intermolecular forces.

FP, for lubricants, is one of the parameters concerning the evaporation tendency and stability after heating, and the higher FP signifies the security and stability during transportation, storage, and use under actual working conditions [29]. Previous studies indicated that FP was related to the vapor pressure of the lubricant at a certain temperature [39]. As the temperature rises, the vapor pressure of the lubricant becomes higher, and part of the chemical bonds connected to high-energy molecules or functional groups tend to break since they have a lower dissociation energy, resulting in the formation of volatiles [40]. As is clear from Fig. 2(d), as the glycol chain length increases, FP increases slowly, which is attributed to the lower dissociation energy of ether bond. Furthermore, as the increase of alkyl chain length, FP increases, which is attributed to the vapor pressure decrease as the intermolecular force increases.

PP, the important parameter of low-temperature fluidity, is the lowest temperature at which the lubricant being cooled can flow. For lubricants, lower PP indicates the wider application at low temperatures. In Fig. 2(e), PPs of OEEs with branched structures are all below -60 °C. For the OEEs with straight-chain structure, alkyl chain length plays a decisive role in the low-temperature flow properties, and PP increases from negative to positive with increasing chain length. Furthermore, it is found that the structure of 4g-2c4 is straight-chain OEEs, with four ether group locating between the molecular short chain, whose low-temperature behavior might resemble of branched-chain OEEs. With increasing glycol chain length for OEEs containing certain straight alkyl chains length, their PP decreases and then increases. The regularity of structure (glycol and alkyl chains length) on PP can be simplified that the branched chain structure is the main factor. Noticeably, increasing the glycol and straight alkyl chain length shows positive contribution, but not always, implying that short straight-chain OEEs still have excellent low-temperature flow performance. In addition to the higher molecular rigidity, we believe that the possible reason is that the molecular polarity of the ether group dominates, resulting in the enhancement the molecule flexibility [41].

Oxidation stability is the ability of a lubricant to resist deterioration due to the combined action of

oxygen, water and metal catalysis, evaluated using OIT. As can be seen in Fig. 2(f), oxidative stability performance is the inferiority for OEEs, deteriorating with increasing glycol chain length. The ether bonds are susceptible to breakage by free radicals and the vulnerable parts of the molecule increase with the glycol chain length, reducing the OIT of OEEs [42]. OITs of straight-chain OEEs are similar with none exceeding 22 minutes, while branched-chain OEEs exhibit a positive effect to some extent. Compared to straight-chain OEEs, OIT of branched-chain OEEs is higher for the same MW, with 2g-2ci8 having the longest OIT of 28 min. The reason is that branching leads to a reduction in chain length and the shorter chains are less susceptible to oxidative cleavage compared to the longer chains [43].

The thermal stability measurements of OEEs based on TGA experiments are shown in Fig. 3. The decomposition temperature of the gradually increases with increasing glycol and alkyl chain length. Table 1 shows the temperatures of OEEs at 10%, 30%, and 50% weight loss. It can be seen that the temperatures of straight-chain and branched-chain OEEs are similar at each weight loss percentage. As the glycol chain length increases, $T_{10\%}$ of 2g-2ci8 is 177 °C, $T_{10\%}$ of 3g-2ci8 is 198 °C, and $T_{10\%}$ of 6g-2ci8 is 253 °C. However, the decomposition temperatures of the OEEs are all below 400 °C, which can be explained by the fact that the electron absorption of the CH_2 unit

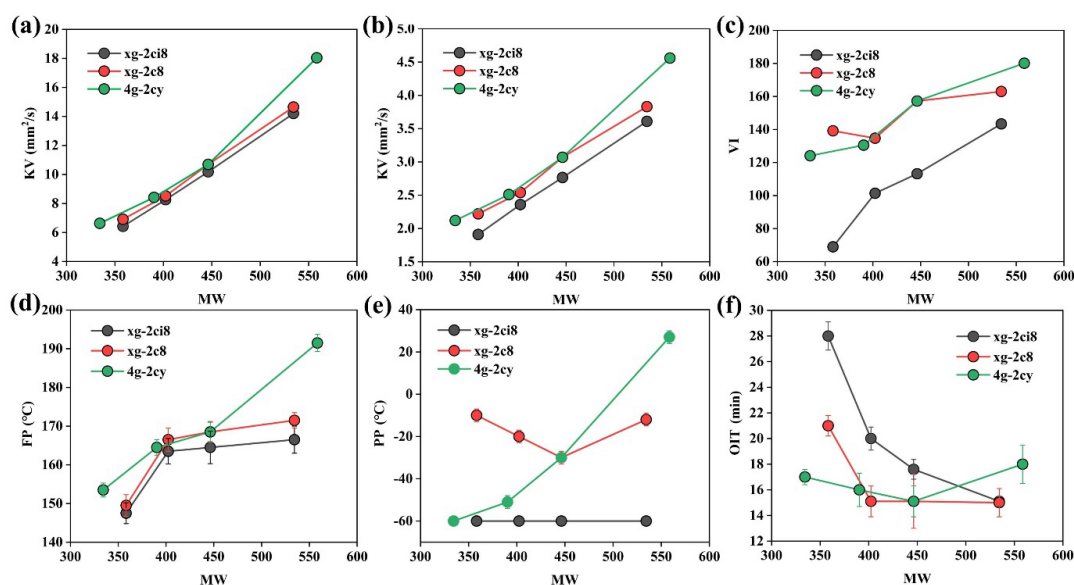


Fig. 2 Conventional properties of OEEs with different structures. (a) KV at 40 °C; (b) KV at 100 °C; (c) VI; (d) FP; (e) PP; (f) OIT.

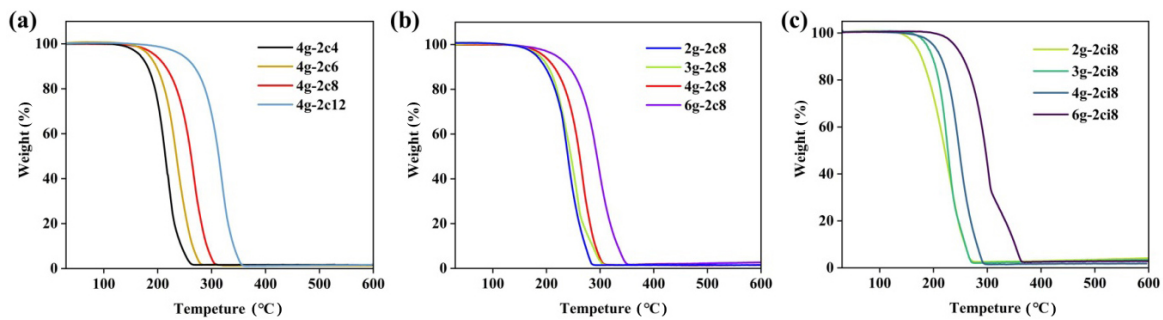


Fig. 3 Variation of thermal stability of OEEs. (a) 4g-2cy series; (b) xg-2c8 series; (c) xg-2ci8 series.

Table 1 $T_{10\%}$, $T_{30\%}$, and $T_{50\%}$ of OEEs.

Lubricant	T_{onset} (°C)	TG temperature (°C) per weight loss			T_{offset} (°C)
		10%	30%	50%	
2g-2c8	186.4	197	227	242	242.6
2g-2ci8	176.5	177	203	221	226.4
3g-2c8	215.6	203	230	246	277.0
3g-2ci8	194.4	198	217	227	232.8
4g-2c4	172.7	181	203	214	216.9
4g-2c6	207.2	197	223	234	291.6
4g-2c8	223.8	214	246	262	323.7
4g-2ci8	215.3	213	236	248	306.4
4g-2c12	298.4	267	299	313	436.3
6g-2c8	260.7	242	278	294	366.2
6g-2ci8	265.3	253	282	297	358.9

3.3 Tribological property

Figure 4(a) shows COF versus sliding time for OEEs (4g-2cy) with different alkyl chain lengths. Compared with 4g-2c4, the oil samples with longer alkyl chains sequentially exhibit a decrease in COF. 4g-2c12 exhibits the smallest COF during sliding, obviously, increasing the length of alkyl chains can provide better lubrication. Previous studies have shown that longer chain molecules can form a thicker oil film on the friction surface to resist shear force [44]. Figures 4(b) and 4(c) show COF of straight-chain OEEs (xg-2c8) and branched-chain OEEs (xg-2ci8) with different glycol chain lengths, respectively. Compared with 2g-2c8, COF of 6g-2c8 decreases significantly by 15%, suggesting that long glycol chains may enhance the lubricating performance by improving the adsorption behaviour. Compared with the two series of OEEs,

attached to the ether bond makes the ether bond susceptible to cleavage or nucleophilic attack [34].

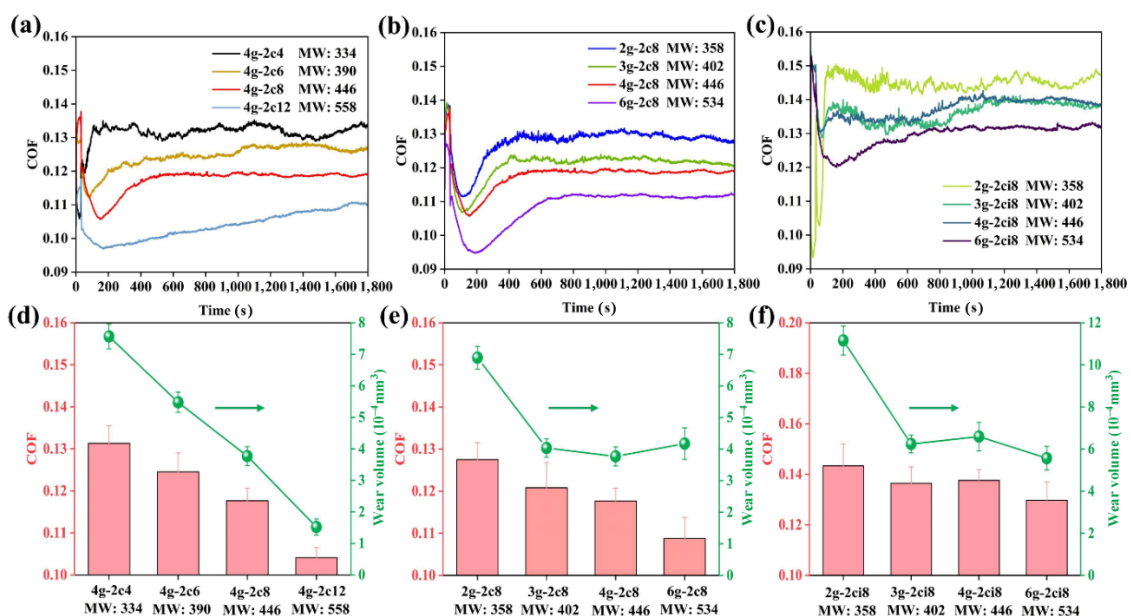


Fig. 4 Evolution of COF (a, b, c) and WV (d, e, f) for OEEs.

xg-2c8 (Fig. 4(b)) and xg-2ci8 (Fig. 4(c)), COF of the mutually isomeric straight and branched-chain OEEs differs significantly, with COF curves of the straight-chain OEEs generally lower than those of branched-chain OEEs, indicating that alkyl structures of the branched chains lead to increased shear force. Average COF and WV are used to quantitatively evaluate the friction reducing and anti-wear performances of OEEs (Figs. 4(d)–4(f)). Compared to 4g-2c4, 4g-2c12 reduces WV from 7.6×10^{-5} to 1.5×10^{-5} mm^3 (Fig. 4(d)). WV of straight and branched OEEs decreases with increasing glycol chain length, however, when the number of glycols increases to 3, the change in WV is minimal (Figs. 4(e) and 4(f)). It indicates that the length of straight alkyl chains is a more effective way to improve anti-wear ability. Furthermore, 3D image of the wear tracks on the disc in Fig. 5 demonstrates the major role of long alkyl chains on the anti-wear performance. Obviously, the increased molecular mass of ester oils will be beneficial for their tribological properties. With the similar molecular structure, the ester with the

highest molecular weight shows the most excellent friction-reducing and anti-wear effect, which may be attributed to the more stable adsorption at the metal interface, as can be confirmed in Fig. 10. In addition, the longer alkyl chains in the structure of the high molecular weight ester oils can provide van der Waals forces to stable the boundary lubricating film formed at the sliding interface, thus slowing down the direct contact between the metal friction pairs.

3.4 Surface analysis

Figure 6 shows SEM images and cross-sectional views of the wear trajectory of the lower disc using 4g-2cy series as lubricants. Under the condition of 4g-2c4 lubrication, significant abrasive wear and adhesive occurs, which is evidenced by severe furrows and surface delamination on the wear area. Due to the lack of a sufficiently thick lubricating film, the furrows and surface delamination are formed by the abrasive removal action on the substrate material and

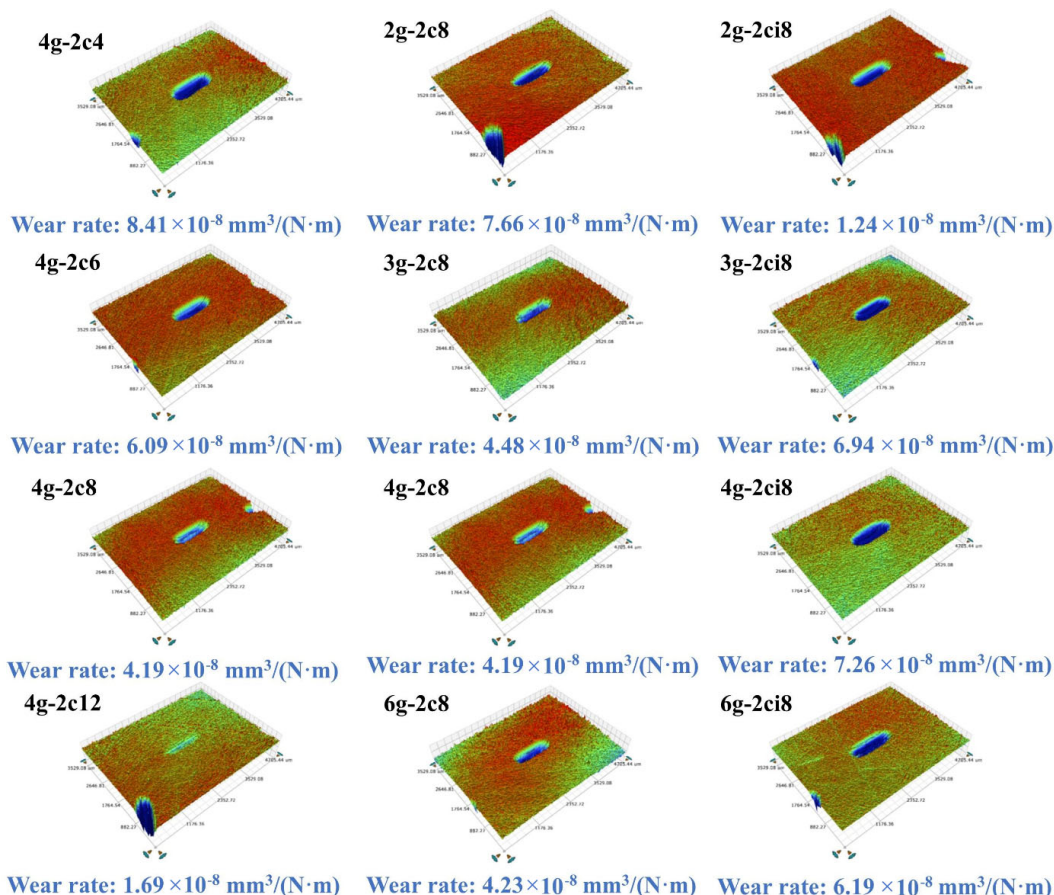


Fig. 5 3D micrographs of wear tracks lubricated by OEEs and the corresponding wear rates.

the cold-welding action between the friction substrates, respectively [45]. Under 4g-2c6 lubrication, a wide range of furrows and surface delamination appear on the wear surface. Compared to the surface lubricated by the 4g-2c4, the width of the furrows lubricated by 4g-2c6 is significantly reduced, while the surface delamination is still evident. After the 4g-2c8 lubricating effect, the slight gouges and spalling pits are observed on the wear surface, indicating a significant improvement in lubrication. As expected, the wear surface with 4g-2c12 has the relatively smooth and reduced abrasive wear, showing the optimal anti-wear capability. Figures 6(a1), 6(b1), 6(c1), and 6(d1) show the maximum depth of the wear trajectory and the width of the cross section as a way to quantitatively assess the anti-wear performance of the 4g-2cy. The width and depth of the wear track continuously

decrease as the alkyl chain length increases. Compared with 4g-2c6, the width of the wear track decreases by 58 μm under 4g-2c8 lubrication and the depth is less than 1.5 μm overall, but the maximum wear depth is greater than 4g-2c6 due to the occurrence of abrasive wear. Under 4g-2c12 lubrication, the width of the wear track is only 418 μm and the maximum depth is 0.53 μm . This indicates that the anti-wear performance is significantly enhanced with the increase of alkyl chain length.

SEM and cross-sectional images of the wear trajectories for xg-2c8 and xg-2ci8 are shown in Figs. 7 and 8, respectively. OEEs with longer glycol chains have improved anti-wear performance in comparison to those with glycol chain length of two, as shown by the significant reduction of groove width and the smoother wear surface. Especially, the wear track

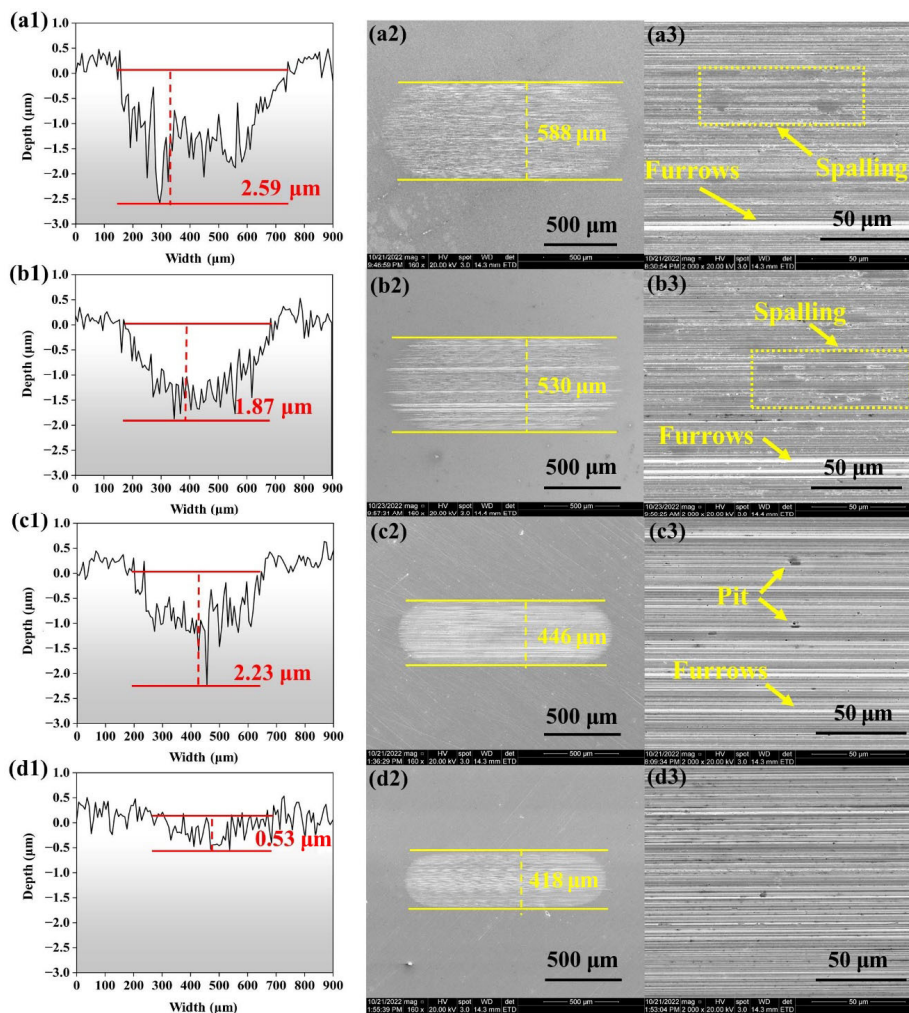


Fig. 6 Characteristics of wear area under 4g-2cy series lubrication: (1) depth curve of cross-section, (2) macroscopic SEM image, (3) local enlarged SEM image; (a) 4g-2c4, (b) 4g-2c6, (c) 4g-2c8, (d) 4g-2c12.

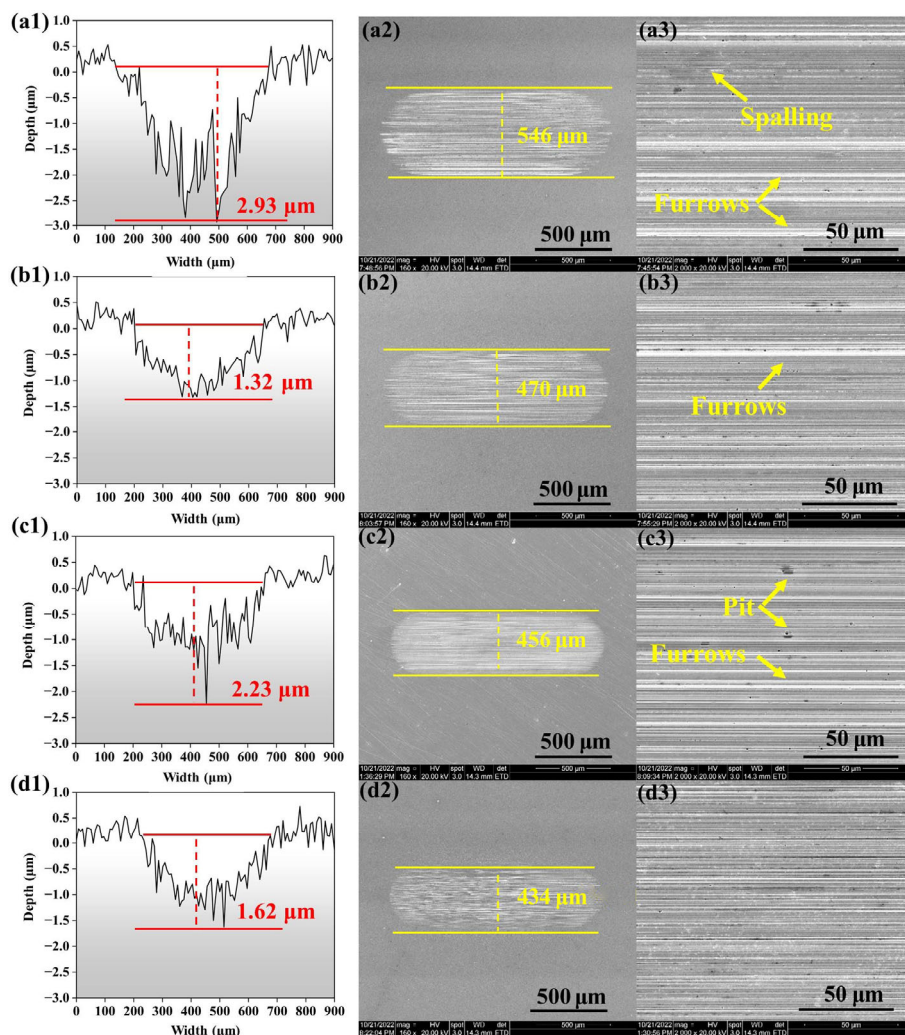


Fig. 7 Characteristics of wear area under xg-2c8 series lubrication: (1) depth curve of cross-section, (2) macroscopic SEM image, (3) local enlarged SEM image; (a) 2g-2c8, (b) 3g-2c8, (c) 4g-2c8, (d) 6g-2c8.

width of 6g-2c8 is reduced by 21% and the maximum wear depth is reduced by 45% compared to 2g-2c8. However, the wear surface improvement with xg-2ci8 lubrication is weaker due to the spatial repulsion of the branched chain structure [44]. Nevertheless, the wear is significantly improved when the numbers of glycol chains grow to 6, demonstrating that longer glycol chains are required for branched-chain OEEs to resist wear in comparison to straight-chain OEEs.

3.5 Wettability analysis

Wettability, the spreading ability of ester oil on iron substrate, is quantified by CA. In the Fig. 9, CA values of three series of OEEs are all less than 20° , indicating the strong interaction with the metal surface, which reduces the interface cohesion of the lubricant molecules.

From Fig. 9(a), the slight increase in CA value is observed with the increase in alkyl chain length, specifically, CA values change from 9.70° (4g-2c4) to 18.24° (4g-2c12). This indicates that the alkyl chain length has the significant effect on CA values. In this process, ester and ether functional groups are adsorbed on the metal surface as polar groups. Owing to the hydrophobic nature of the alkyl chains, the longer alkyl chain portion of OEEs at the tail leads to the increased intermolecular interactions [19, 46] and therefore CA increases with the alkyl chain length. Similarly, in Figs. 9(b) and 9(c), compared with the inferior wettability to xg-2ci8 series esters (CA is about 9° – 11°), CAs between the xg-2c8 series are close to 17° – 18° . Usually, the symmetry of oxygen atoms increases the hydrophobicity of lubricant molecules

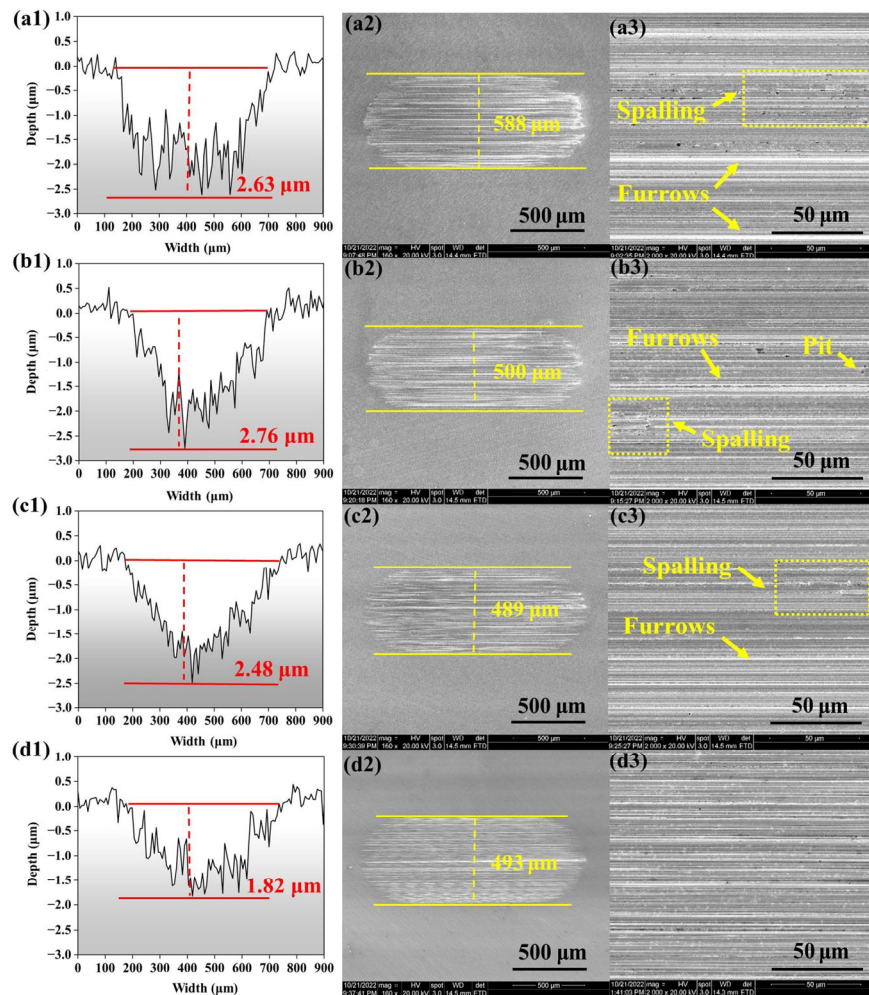


Fig. 8 Characteristics of wear area under xg-2c8 series lubrication: (1) depth curve of cross-section, (2) macroscopic SEM image, (3) local enlarged SEM image: (a) 2g-2ci8, (b) 3g-2ci8, (c) 4g-2ci8, (d) 6g-2ci8.

[47], but here, the numbers of ether groups show the weak effect on reducing the molecular cohesion energy. Obviously, the wettability depends mainly on the alkyl chains structure to the certain extent. Different from the influence of straight alkyl side chains, branched chains have weak intermolecular interaction forces with preferable wettability.

3.6 Adsorption analysis

A QCM-D is used to further evaluate the adsorption capacity of OEEs on the gold chip in the Fig. 10. After washing with ethanol at the end of the test, Δf and ΔD return to the initial value of 0, which indicates that the physical adsorption is dominant. As shown in Figs. 10(a1), 10(a2), and 10(a3), Δf decreases with increasing alkyl chain length, while ΔD increases regularly. As for the influence of the length of glycol

chain in OEEs on adsorption, a positive contribution is evident (Figs. 10(b) and 10(c)). It is notable that the results also correspond to the previous friction test as shown in Fig. 4, demonstrating that OEEs with long alkyl and glycol chains have stronger adsorption and will exhibit better lubrication properties. Comparing the three series of OEEs, 4g-2c12 exhibits the strongest adsorption capacity with the smallest Δf and the largest ΔD . Besides, the consideration on the MW concerning their adsorption capacity is essential. Intriguingly, MW of 4g-2c4 is much smaller than that of 2g-2c8 and 2g-2ci8, but the Δf is ranked as 4g-2c4 (28.5 Hz) < 2g-2c8 (28.3 Hz) < 2g-2ci8 (24.7 Hz). It indicates that the effect of ether functional groups on the adsorption capacity is not negligible.

Schematic diagram of adsorption is shown in Fig. 11 to facilitate the understanding of the adsorption

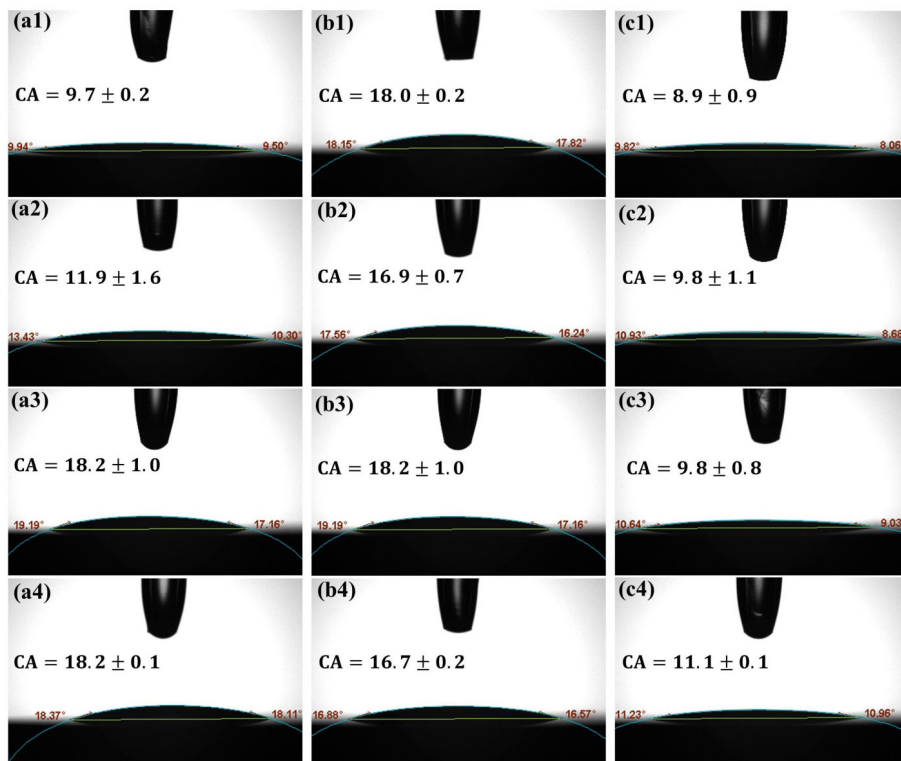


Fig. 9 CA of 3 series of lubricants. (a1–a4) 4g-2cy series; (b1–b4) xg-2c8 series; (c1–c4) xg-2ci8 series.

behavior of OEEs at the interface. The polar ester and ether functional groups are adsorbed on the gold sheet to different degrees when the lubricant molecules flow with the ethanol solvent on the surface of the sheet, while the alkyl chains on both sides are perpendicular to the gold sheet surface under the stretching effect of the polar groups and the intermolecular Van der Waals forces. The adsorption sites are more and the adsorption capacity is stronger as the number of ether functional groups in the lubricant molecule increases, so Δf decreases regularly, while ΔD increases regularly (Fig. 11(a)). With the same number of ether functional groups, Δf and ΔD depend on the length of the alkyl chain, with longer chain alkyl groups having greater MW and therefore greater adsorption mass (Fig. 11(b)). Compared to straight alkyl side chains, the ΔD of branched alkyl side chains is lower than that of straight alkyl OEEs with the same MW because they yield greater spatial site resistance (Fig. 11(c)). 4g-2c4 is half the length of the straight alkyl of 2g-2c8, however, its Δf and ΔD are similar to that of 2g-2c8 because it adsorbs more molecules due to less spatial site resistance.

3.7 XPS and Raman analysis

The elemental and chemical states of the wear regions of the three OEEs with superior lubrication are analyzed using XPS. As shown in Figs. 12(a), 12(b), and 12(c), XPS spectra figures are 4g-2c12, 6g-2c8, and 6g-2ci8, respectively. Three peaks of C1s at around 284.8, 286, and 288.4 eV correspond to C–C, C–O, and C=O [19], respectively. Three peaks of O1s are located at 529.7, 531.4, and 523.5 eV, corresponding to FeO, C–O, and O–H bonds [48], respectively. XPS peaks of Fe2p appear at 710.2 and 723.3 eV, which, in combination with the peak positions of O1s, may be due to the production of the compounds Fe_2O_3 and Fe_3O_4 [49]. The peak of Fe2p at 713 eV may be due to the production of FeOOH and Fe(OH)O [50]. To further evaluate the composition of the interfacial film formed on the iron substrate, Raman testing is employed at the wear region lubricated by esters. In Fig. 13, the peak at 664 cm^{-1} is attributed to Fe_3O_4 [51]. In addition, the characteristic peaks of graphite at $1,349$ and $1,573\text{ cm}^{-1}$ [52] are labeled in the figure. The results indicate that the main components detected on the friction surface are Fe_3O_4 and carbonaceous

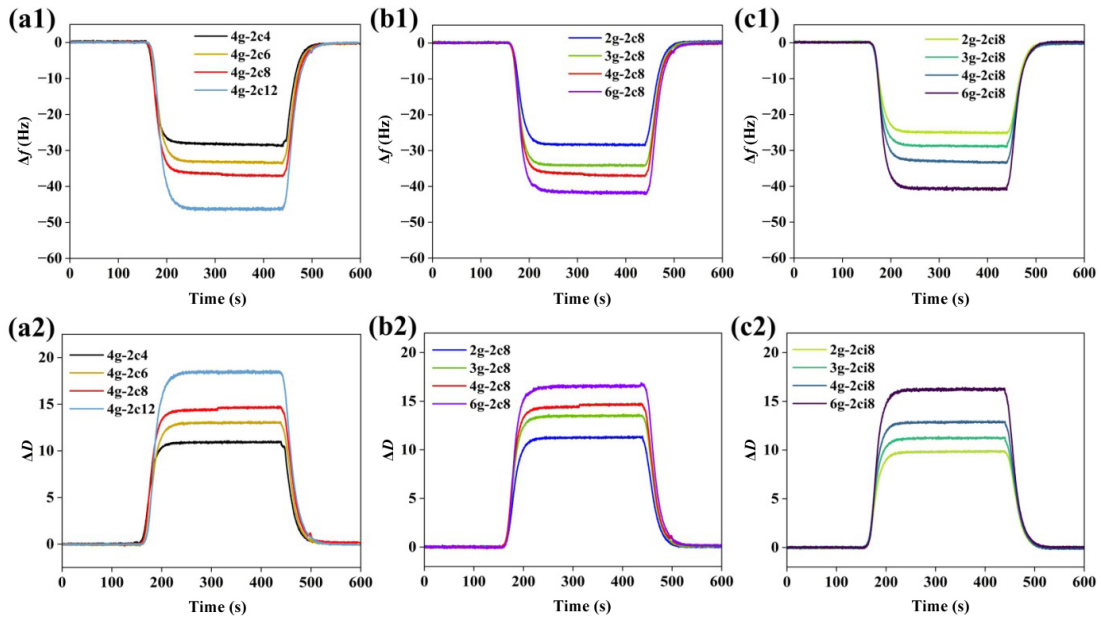


Fig. 10 Frequency (Δf) of OEEs. (a1) 4g-2cy series; (b1) xg-2c8 series; (c1) xg-2ci8 series. Dissipation (ΔD) of OEEs. (a2) 4g-2cy series; (b2) xg-2c8 series; (c2) xg-2ci8 series.

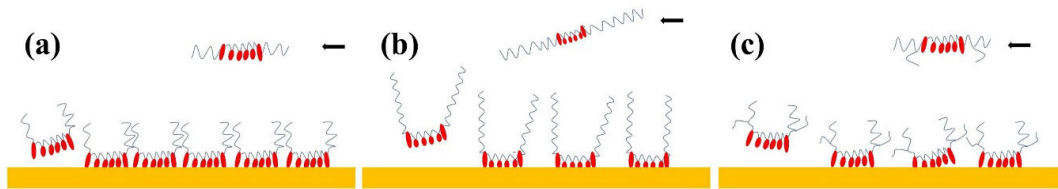


Fig. 11 Schematic diagram of the adsorption mechanism of OEEs with different structures: (a) short alkyl side chains, (b) long alkyl side chains, (c) branched alkyl side chains.

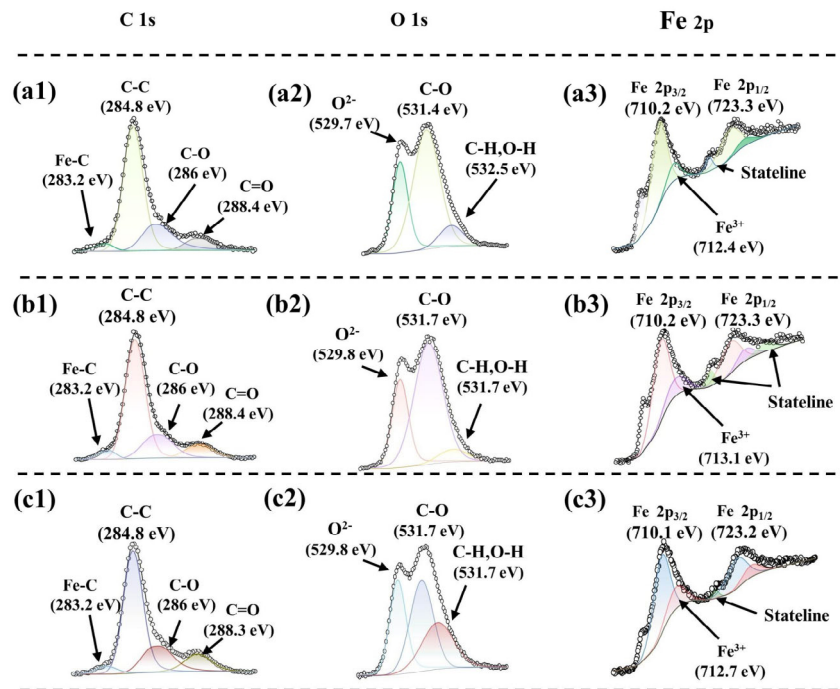


Fig. 12 XPS in the grinding pit area: (1) C 1s, (2) O 1s, (3) Fe 2p; (a) 4g-2c12, (b) 6g-2c8, (c) 6g-2ci8.

material. Undoubtedly, these peaks indicate that oxidation reactions occur at the sliding asperity during friction, while long chain molecules break under high pressure and shear, resulting in the generation and accumulation of the carbonaceous substances. In the well-lubricated (4g-2c12, 6g-2c8, and 6g-2ci8) wear areas, the Raman spectra present the significant peaks of carbonaceous material, which may be the result of the generation tribo-film composed of carbonaceous material at the friction interface [50, 53]. Besides, the minor abrasive chip mixing and doping at the interface act as a solid lubricant [52], such mechanism improves the lubrication. In areas of severe wear under 4g-2c4, 2g-2c8 and 2g-2ci8 lubrication, no carbonaceous peaks were evident. This may be due to the light molecular mass and low boiling point of these lubricants, making the carbon chains break more easily under mechanical shear and extrusion to generate volatile substances (hydrogen and gaseous hydrocarbons) [54]. This leads to their poor anti-wear performance. In the process of friction, new iron surfaces are constantly formed, therefore the peaks of iron oxides are also very weak.

4 Correlation between molecular descriptors and properties

4.1 PCA analysis

PCA is a dimensionality reduction method that transforms complex original data into new orthogonal variables without losing the original information [55, 56]. In visual analysis, a 2D plot of the sample is usually constructed based on the first and second principal components, and 3D plot is constructed with the first three principal components [57]. PCA

scatter plot gives a visual indication of the similarity among the samples. When the points of several samples are clustered together, it means that there is a high similarity among these samples. Conversely, if the sample points are scattered, it indicates that the similarity among them is relatively low. PCA method has been applied in many fields, such as determining the classes of air pollutants [58, 59], distinguishing the homologue groups of chlorinated paraffins [60] and the different kinds of asphalt [56].

PCA was conducted for all molecular descriptors to determine the ideal molecular descriptor. As shown in Fig. 14(a), OEEs are clustered in two different regions (black and red circles) in 2D pot, where the black scatters represent straight-chain OEEs and the red scatters represent branched OEEs. The clustering trend of scatters indicates that, for straight-chain and branched-chain OEEs, there is a lot of duplication of structural information of molecules within each group, while there are significant differences in the structural information between the two groups. As shown in Fig. 14(b), OEEs with different glycol chain lengths have clear spatial trajectories in 3D plot. Furthermore, OEEs with different alkyl chain lengths, such as 4g-2c4, 4g-2c6, 4g-2c8, and 4g-2c12, can also be identified, and they have different heights in PC3 direction, but have similar projections under PC1 and PC2. The first, second, and third principal components explain 95.3% of the structural information, while PC1, PC2, and PC3 explain 43.2%, 33.1% and 19%, respectively. To conclude, the identification of these two structures of OEEs is important for the construction of PLS models.

Correlations between the 13 molecular descriptors screened and various properties of OEEs were investigated using PCA, and the results are presented

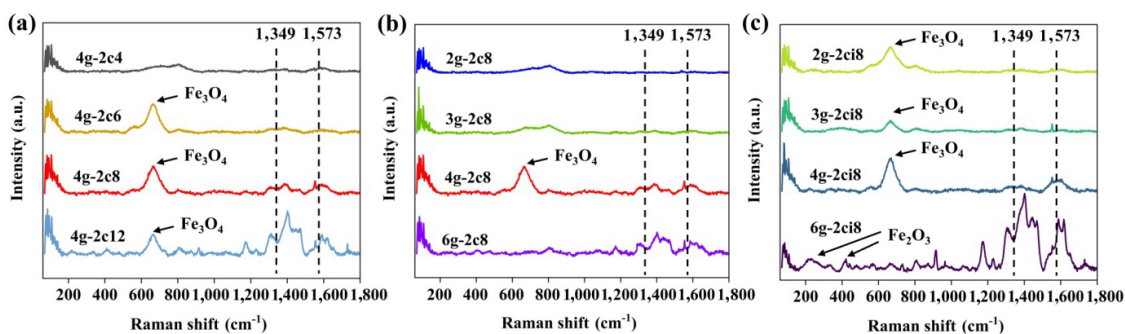


Fig. 13 Raman spectra of wear scar. (a) 4g-2c12; (b) 6g-2c8; (c) 6g-2ci8.

in Fig. 15 in the form of correlation circle plots. The influence of the molecular descriptors on the properties is mainly seen in the length and orientation of the lines. Larger lengths indicate a greater effect on the

observed terms. The angle between the lines reflects the correlation between them; the smaller the angle, the closer their correlation coefficient is to 1. When the angle is 90 or 270 degrees, they are not correlated

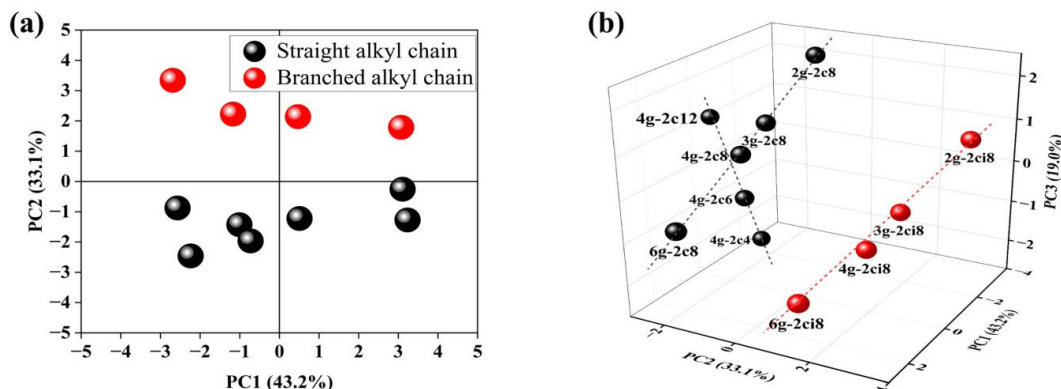


Fig. 14 PCA results of samples. (a) 2D score plot; (b) 3D score plot.

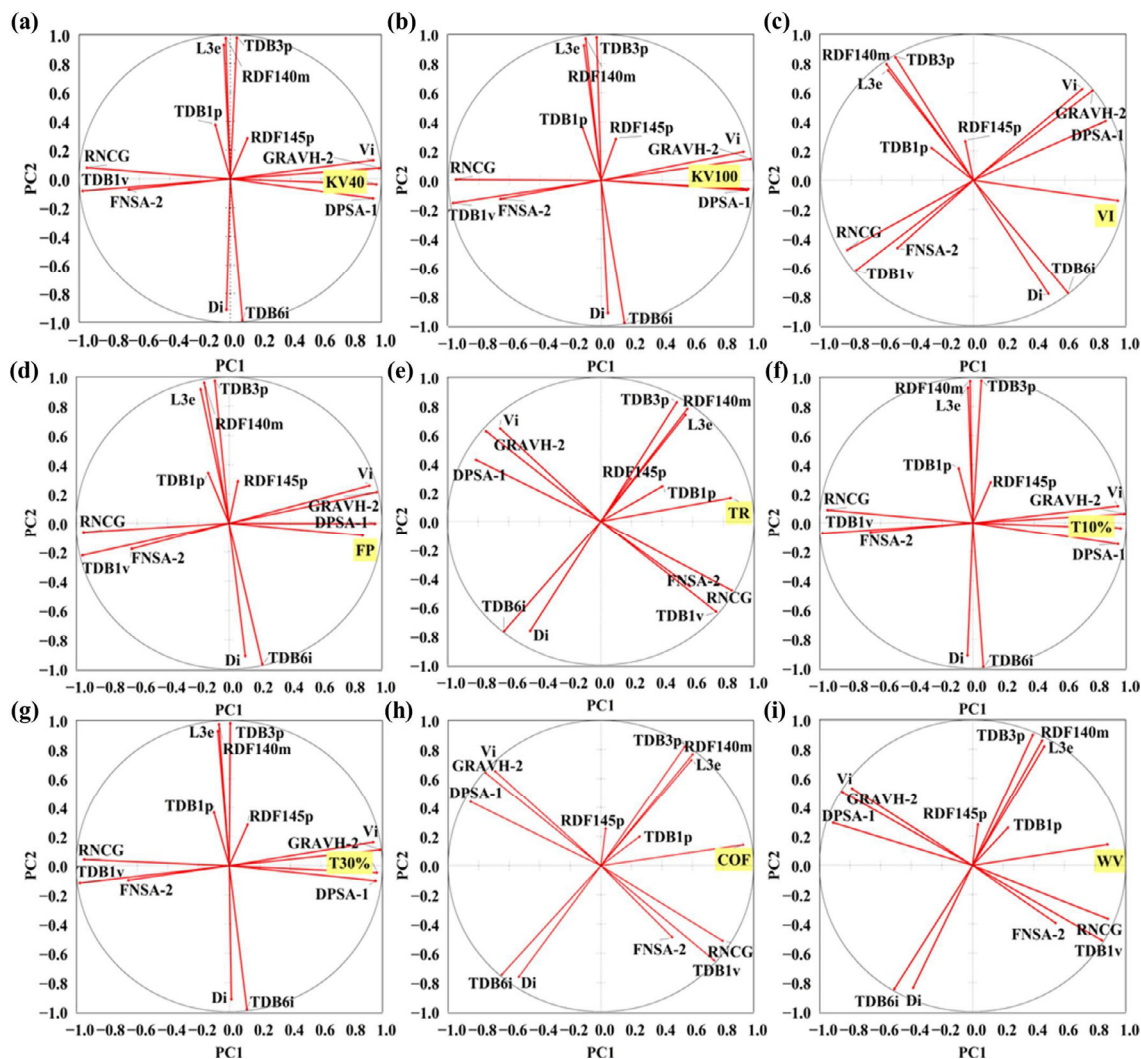


Fig. 15 Correlation circle graph. (a) KV at 40 °C; (b) KV at 100 °C; (c) VI; (d) OIT; (e) PP; (f) $T_{10\%}$; (g) $T_{30\%}$; (h) COF; (i) WV.

and the correlation coefficient is 0. When the angle is 180, they are negatively correlated and the correlation coefficient is -1 .

4.2 PLS analysis

PLS is a multivariate linear statistical model that predicts the output variable Y from the input variable X [61]. The calibrated models based on molecular descriptors were developed using PLS for all lubricants with similar structures. In order to determine the best model results for each property of OEEs, different principal fractions were compared to avoid underfitting due to small principal fractions or overfitting due to large principal fractions. In addition, cross-validation (leave-one-out method) is used to verify the generalization ability of the model. For the leave-one-out method, only one data in the dataset is used at one time as validation, and the rest of the data are used for prediction. As a result, the best models for the physical-chemical and tribological properties of OEEs are determined, as shown in Table 2.

The R^2 and RMSE between the experimental and predictive values are used to assess the validity of the model. Generally, when $R^2 > 0.7$, it indicates that the predictive value has the potential ability to replace the experimental value.

Figure 16 exhibits the loss between the experimental and predictive values for various properties of OEEs. It can be observed that the molecular descriptors have good modeling capability. Among them, the tribological properties are most satisfactorily evaluated

with R^2 close to 0.9 for COF and WV, followed by thermal stability with R^2 higher than 0.84. Among the conventional properties, R^2 for viscosity–temperature properties are above 0.8, however, FP and oxidation stability properties do not perform well on the test data set. R^2 is smaller, around 0.5.

5 Conclusions

As a direction in the development of low-viscosity lubricants, the molecular structure of OEEs determines their physicochemical properties and impacts their friction and wear performances during the sliding process. Compared with previous ester lubricants, OEEs have the advantages of simple synthesis, lower viscosity, and more importantly, excellent adsorption capacity on steel surfaces. OEEs with different structures exhibit different lubricating effects. Longer glycol and alkyl chain will favor viscosity-temperature properties, thermal-oxidative stability, and tribological properties. Branching structures have poor frictional effect due to the effect of spatial site resistance, but have excellent low temperature fluidity. For the analysis of the worn surfaces, it is shown that the effect of long alkyl and glycol chains on the tribological properties is attributed to the thickness of the adsorbed film and the surface coverage, respectively. Furthermore, the predictive model based on QSPR can accurately evaluate the tribological properties of OEEs, with an R^2 of about 0.9, which can be effectively applied to the development and application of OEEs lubricants.

Table 2 R^2 and RMSE values of the best models.

Group	Predicting parameter	Principal component	R^{2a}	RMSE ^a	R^{2b}	RMSE ^b
Conventional properties	KV@40 °C	2	0.9203	1.0252	0.856	1.0252
	KV@100 °C	3	0.9631	0.1508	0.8551	0.2989
	VI	3	0.9395	7.1976	0.8245	12.2603
	FP	4	0.8696	4.1295	0.5249	7.8810
	OIT	3	0.7843	1.7288	0.4632	2.7269
Thermal stability	$T_{10\%}$	3	0.9542	5.9560	0.8486	10.8256
	$T_{30\%}$	3	0.9713	5.2520	0.9056	20.884
Tribological performance	COF	3	0.9606	0.0023	0.8906	0.0038
	WV	5	0.9908	0.2278	0.9191	0.6762

^atraining model results; ^bcross validation results using the leave-one-out method.

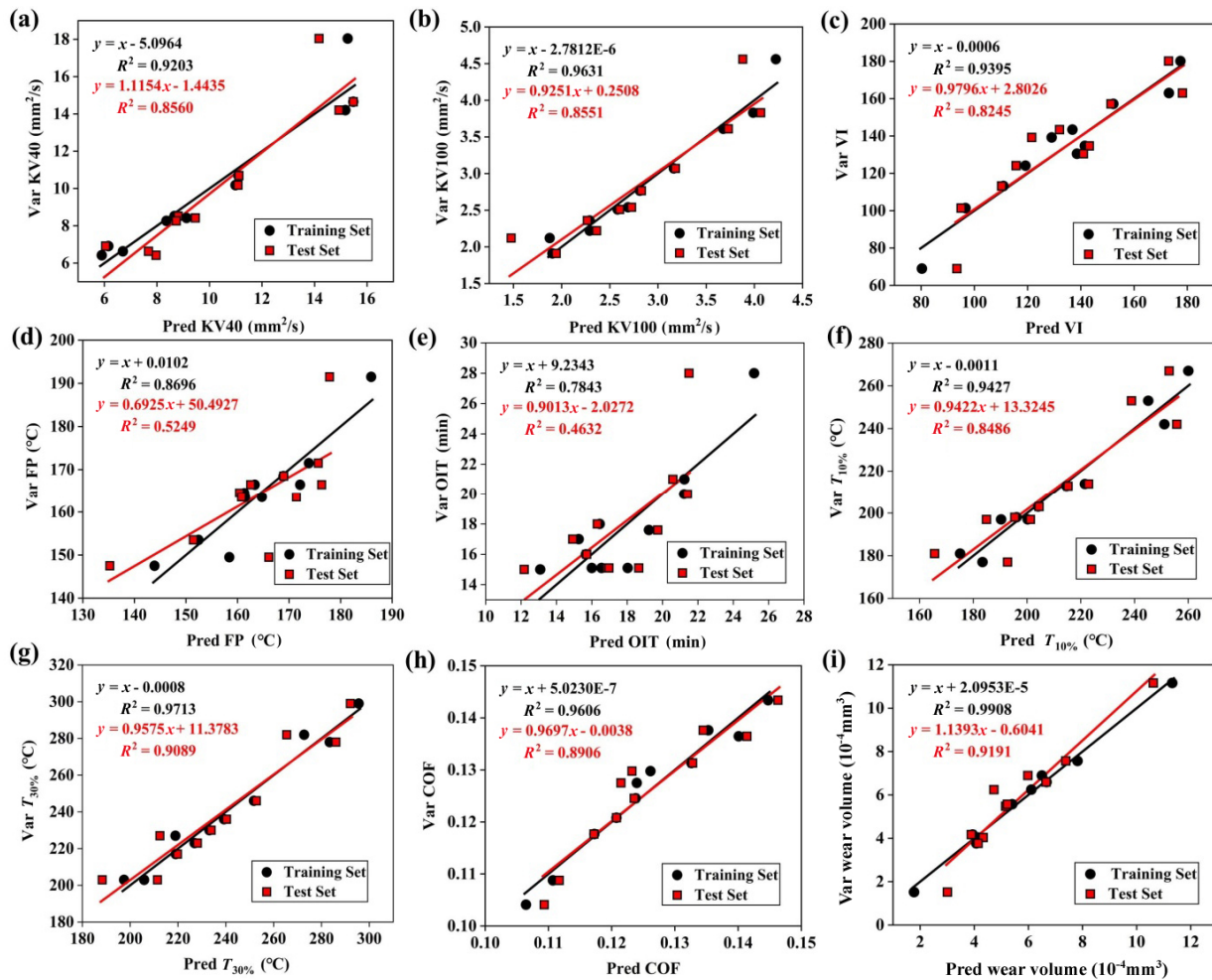


Fig. 16 Results of the best model for the studied lubricating performance. Black indicates training data and red indicates test data. (a) KV at 40 °C; (b) KV at 100 °C; (c) VI; (d) OIT; (e) PP; (f) $T_{10\%}$; (g) $T_{30\%}$; (h) COF; (i) WV.

Acknowledgements

The authors are greatly appreciating the financial supported by the National Natural Science Foundation of China (No. 52175156), the Key Research and Development Projects of Shaanxi Province (No. 2021GY-157), and the Young Talent fund of University Association for Science and Technology in Shaanxi (No. 20220615). This work was also supported by the Special Fund for Basic Scientific Research of Central Colleges (Chang'an University) with Nos. 300102221512, 300102221510, and 300102222502.

Declaration of competing interest

The authors have no competing interests to declare that are relevant to the content of this article.

Electronic Supplementary Material

Supplementary material is available in the online version of this article at <https://doi.org/10.1007/s40544-023-0765-3>.

Open Access This article is licensed under a Creative Commons Attribution 4.0 International License, which permits use, sharing, adaptation, distribution and reproduction in any medium or format, as long as you give appropriate credit to the original author(s) and the source, provide a link to the Creative Commons licence, and indicate if changes were made.

The images or other third party material in this article are included in the article's Creative Commons licence, unless indicated otherwise in a credit line to the material. If material is not included in the article's

Creative Commons licence and your intended use is not permitted by statutory regulation or exceeds the permitted use, you will need to obtain permission directly from the copyright holder.

To view a copy of this licence, visit <http://creativecommons.org/licenses/by/4.0/>.

References

- [1] Holmberg K, Erdemir A. The impact of tribology on energy use and CO₂ emission globally and in combustion engine and electric cars. *Tribol Int* **135**: 389–396 (2019)
- [2] Souza de Carvalho M J, Rudolf Seidl P, Pereira Belchior C R, Ricardo Sodré J. Lubricant viscosity and viscosity improver additive effects on diesel fuel economy. *Tribol Int* **43**(12): 2298–2302 (2010)
- [3] Wong V W, Tung S C. Overview of automotive engine friction and reduction trends—Effects of surface, material, and lubricant-additive technologies. *Friction* **4**(1): 1–28 (2016)
- [4] Vaitkunaite G, Espejo C, Wang C, Thiébaud B, Charrin C, Neville A, Morina A. MoS₂ tribofilm distribution from low viscosity lubricants and its effect on friction. *Tribol Int* **151**: 106531 (2020)
- [5] Gan Z T, Yao T, Zhang M, Hu J Q, Liao X X, Shen Y L. Effect of temperature on the composition of a synthetic hydrocarbon aviation lubricating oil. *Materials* **13**(7): 1606 (2020)
- [6] Martins R C, Fernandes C M C G, Seabra J H O. Evaluation of bearing, gears and gearboxes performance with different wind turbine gear oils. *Friction* **3**(4): 275–286 (2015)
- [7] Zhou C, Tan L, Hu W J, Li J S. A modified oil-soluble polyether used as multifunctional ashless additives with enhanced lubricating and corrosion protection performance. *J Appl Polym Sci* **138**(14): 50134 (2021)
- [8] Belhocine T, Forsyth S A, Nimal Gunaratne H Q, Nieuwenhuyzen M, Puga A V, Seddon K R, Srinivasan G, Whiston K. New ionic liquids from azepane and 3-methylpiperidine exhibiting wide electrochemical windows. *Green Chem* **13**(1): 59–63 (2011)
- [9] Zubeir L F, Spyriouni T, Roest D, Hill J R, Kroon M C. Effect of oxygenation on carbon dioxide absorption and thermophysical properties of ionic liquids: Experiments and modeling using electrolyte PC-SAFT. *Ind Eng Chem Res* **55**(32): 8869–8882 (2016)
- [10] Gan Z Y, Qu S, Li S J, Tan T W, Yang J. Facile synthesis of PET-based poly(ether ester)s with striking physical and mechanical properties. *React Funct Polym* **164**: 104936 (2021)
- [11] Haernvall K, Zitzenbacher S, Yamamoto M, Schick M B, Ribitsch D, Guebitz G. Polyol structure and ionic moieties influence the hydrolytic stability and enzymatic hydrolysis of bio-based 2, 5-furandicarboxylic acid (FDCA) copolyesters. *Polymers* **9**(12): 403 (2017)
- [12] Bantchev G B, Cermak S C. Correlating viscosity of 2-ethylhexyl oleic estolide esters to their molecular weight. *Fuel* **309**: 122190 (2022)
- [13] Poissonnier J, Ranga C, Lødeng R, Thybaut J W. Oxygen functionality and chain length effects in HDO: Impact of competitive adsorption on reactivity. *Fuel* **308**: 121940 (2022)
- [14] Cyriac F, Tee X Y, Poornachary S K, Chow P S. Influence of structural factors on the tribological performance of organic friction modifiers. *Friction* **9**(2): 380–400 (2021)
- [15] Su Y H, Yu J R, Wang Y, Zhu J, Hu Z M. Effect of hard segment length on the properties of poly(ether ester) elastomer prepared by one pot copolymerization of poly(ethylene glycol) and cyclic butylene terephthalate. *J Polym Res* **22**(10): 1–10 (2015)
- [16] Raof N A, Yunus R, Rashid U, Azis N, Yaakub Z. Effect of molecular structure on oxidative degradation of ester based transformer oil. *Tribol Int* **140**: 105852 (2019)
- [17] Zhang J, Tan A, Spikes H. Effect of base oil structure on elasto-hydrodynamic friction. *Tribol Lett* **65**(1): 13 (2017)
- [18] Airey J, Spencer M, Greenwood R, Simmons M. The effect of gas turbine lubricant base oil molecular structure on friction. *Tribol Int* **146**: 106052 (2020)
- [19] Yan Q Q, Ma H J, Dong R, Yan Y Y, Wen P, Fan M J. Salicylate ester derivatives as lubricant: Synergism of multiple interactions to improve tribological performances. *Tribol Int* **169**: 107489 (2022)
- [20] Wang Y R, Yu Q L, Ma Z F, Huang G W, Cai M R, Zhou F, Liu W M. Significant enhancement of anti-friction capability of cationic surfactant by phosphonate functionality as additive in water. *Tribol Int* **112**: 86–93 (2017)
- [21] Shirani A, Joy T, Lager I, Yilmaz J L, Wang H L, Jeppson S, Cahoon E B, Chapman K, Stymne S, Berman D. Lubrication characteristics of wax esters from oils produced by a genetically-enhanced oilseed crop. *Tribol Int* **146**: 106234 (2020)
- [22] Li R Z, Herreros J M, Tsolakis A, Yang W Z. Machine learning-quantitative structure property relationship (ML-QSPR) method for fuel physicochemical properties prediction of multiple fuel types. *Fuel* **304**: 121437 (2021)
- [23] Kang X J, Qian J G, Deng J, Latif U, Zhao Y S. Novel molecular descriptors for prediction of H₂S solubility in ionic liquids. *J Mol Liq* **265**: 756–764 (2018)



- [24] Yin N, Xing Z G, He K, Zhang Z N. Tribo-informatics approaches in tribology research: A review. *Friction* **11**(1): 1–22 (2023)
- [25] Hosseinpour S, Aghbashlo M, Tabatabaei M. Biomass higher heating value (HHV) modeling on the basis of proximate analysis using iterative network-based fuzzy partial least squares coupled with principle component analysis (PCA-INFPLS). *Fuel* **222**: 1–10 (2018)
- [26] Wan Z Y, Wang Q D, Liu D C, Liang J H. Discovery of ester lubricants with low coefficient of friction on material surface via machine learning. *Chem Phys Lett* **773**: 138589 (2021)
- [27] Nasab S G, Semnani A, Marini F, Biancolillo A. Prediction of viscosity index and pour point in ester lubricants using quantitative structure-property relationship (QSPR). *Chemom Intell Lab Syst* **183**: 59–78 (2018)
- [28] Hong F T, Ladelta V, Gautam R, Sarathy S M, Hadjichristidis N. Polyether-based block co(ter)polymers as multifunctional lubricant additives. *ACS Appl Polym Mater* **3**(8): 3811–3820 (2021)
- [29] Hu C H, He X, Han Y Y, Ye X Y, Fan M J, Zhou F, Liu W M. High performance lubricants prepared from Naphthalene-1, 4,5,8-Tetracarboxylic acid: Synthesis, physicochemical and Tribological properties. *J Mol Liq* **330**: 115609 (2021)
- [30] Fan M J, Ai J, Zhang S, Yang C L, Du X, Wen P, Ye X Y, Zhou F, Liu W M. Lubricating properties of ester oil prepared from bio-based 2,5-furandicarboxylic acid. *Friction* **8**(2): 360–369 (2020)
- [31] Wang W, Zhang G L, Xie G X. Ultralow concentration of graphene oxide nanosheets as oil-based lubricant additives. *Appl Surf Sci* **498**: 143683 (2019)
- [32] Dong J, Cao D S, Miao H Y, Liu S, Deng B C, Yun Y H, Wang N N, Lu A P, Zeng W B, Chen A F. ChemDes: An integrated web-based platform for molecular descriptor and fingerprint computation. *J Cheminform* **7**: 60 (2015)
- [33] Zojaji I, Esfandiarian A, Taheri-Shakib J. Toward molecular characterization of asphaltene from different origins under different conditions by means of FT-IR spectroscopy. *Adv Colloid Interface Sci* **289**: 102314 (2021)
- [34] Chen Z J, Huo Y N, Cao J, Xu L, Zhang S G. Physicochemical properties of ether-functionalized ionic liquids: Understanding their irregular variations with the ether chain length. *Ind Eng Chem Res* **55**(44): 11589–11596 (2016)
- [35] Rahim A H A, Yunus N M, Hamzah W S W, Sarwono A, Muhammad N. Low-viscosity ether-functionalized ionic liquids as solvents for the enhancement of lignocellulosic biomass dissolution. *Processes* **9**(2): 261 (2021)
- [36] Zhang C H, Wang H W, Yu X W, Peng C L, Zhang A G, Liang X M, Yan Y N. Correlation between the molecular structure and viscosity index of CTL base oils based on ridge regression. *ACS Omega* **7**(22): 18887–18896 (2022)
- [37] Hemmat Esfe M, Abbasian Arani A A, Esfandeh S. Experimental study on rheological behavior of monograde heavy-duty engine oil containing CNTs and oxide nanoparticles with focus on viscosity analysis. *J Mol Liq* **272**: 319–329 (2018)
- [38] Ting C C, Chen C C. Viscosity and working efficiency analysis of soybean oil based bio-lubricants. *Measurement* **44**(8): 1337–1341 (2011)
- [39] Xu T, Shi H Q, Wang H, Huang X M. Dynamic evolution of emitted volatiles from thermal decomposed bituminous materials. *Constr Build Mater* **64**: 47–53 (2014)
- [40] Vedharaj S, Vallinayagam R, Sarathy S M, Dibble R W. Improving vegetable oil fueled CI engine characteristics through diethyl ether blending. In *ASME 2016 Internal Combustion Engine Fall Technical Conference ICEF2016-9339* (2016)
- [41] Zhou Z B, Matsumoto H, Tatsumi K. Low-melting, low-viscous, hydrophobic ionic liquids: 1-alkyl(alkyl ether)-3-methylimidazolium perfluoroalkyltrifluoroborate. *Chem Eur J* **10**(24): 6581–6591 (2004)
- [42] Chen J C, Chen P Y, Liu Y C, Chen K H. Polybenzimidazoles containing bulky substituents and ether linkages for high-temperature proton exchange membrane fuel cell applications. *J Membr Sci* **513**: 270–279 (2016)
- [43] Yasa S R, Cheguru S, Krishnasamy S, Korlipara P V, Rajak A K, Penumarthy V. Synthesis of 10-undecenoic acid based C₂₂-dimer acid esters and their evaluation as potential lubricant basestocks. *Ind Crops Prod* **103**: 141–151 (2017)
- [44] Cyriac F, Yamashita N, Hirayama T, Yi T X, Poornachary S K, Chow P S. Mechanistic insights into the effect of structural factors on film formation and tribological performance of organic friction modifiers. *Tribol Int* **164**: 107243 (2021)
- [45] Kerni L, Raina A, Haq M I U. Friction and wear performance of olive oil containing nanoparticles in boundary and mixed lubrication regimes. *Wear* **426–427**: 819–827 (2019)
- [46] de Paula F H M, de Freitas F A, Nunes D G, Iglauer S, Gramatges A P, Nascimento R S V, Lachter E R. Alkyl glyceryl ethers as water-based lubricant additives in mixtures with xanthan gum. *Colloids Surf A* **634**: 127881 (2022)
- [47] Dharmaratne N, Jouaneh T M M, Kiesewetter M K, Mathers R T. Quantitative measurements of polymer hydrophobicity based on functional group identity and oligomer length. *Macromolecules* **51**(21): 8461–8468 (2018)
- [48] Niu Y X, Pang X J, Yue S W, Shangguan B, Zhang Y Z. The friction and wear behavior of laser textured surfaces in non-conformal contact under starved lubrication. *Wear* **476**: 203723 (2021)

- [49] Zhang J Y, Bao L Y, Yu Q L, Ma Z F, Dong R, Zhang C Y, Bai Y Y, Cai M R, Zhou F, Liu W M. Gelation mechanism and tribological performances of two-component cholesterol-based supramolecular gel lubricant. *Tribol Int* **155**: 106777 (2021)
- [50] Yu H X, Chen H J, Zheng Z W, Qiao D, Feng D P, Gong Z B, Dong G J. Effect of functional groups on tribological properties of lubricants and mechanism investigation. *Friction* **11**(6): 911–926 (2023)
- [51] Saini V, Seth S, Ramakumar S S V, Bijwe J. Carbon nanoparticles of varying shapes as additives in mineral oil assessment of comparative performance potential. *ACS Appl Mater Interfaces* **13**(32): 38844–38856 (2021)
- [52] Yu H X, Chen H J, Zheng Z W, Ba Z W, Qiao D, Feng D P, Gong Z B, Dong G J. Transformation mechanism between the frictional interface under dioctyl sebacate lubrication. *Tribol Int* **155**: 106745 (2021)
- [53] Zheng D D, Su T, Ju C. Influence of ecofriendly protic ionic liquids on the corrosion and lubricating properties of water-glycol. *Tribol Int* **165**: 107283 (2022)
- [54] Lu R G, Minami I, Nanao H, Mori S. Investigation of decomposition of hydrocarbon oil on the nascent surface of steel. *Tribol Lett* **27**(1): 25–30 (2007)
- [55] Benguerba Y, Alnashef I M, Erto A, Balsamo M, Ernst B. A quantitative prediction of the viscosity of amine based DESs using $S\sigma$ -profile molecular descriptors. *J Mol Struct* **1184**: 357–363 (2019)
- [56] Xu M, Zhang Y Z, Zhao P H, Liu C. Study on aging behavior and prediction of SBS modified asphalt with various contents based on PCA and PLS analysis. *Constr Build Mater* **265**: 120732 (2020)
- [57] Granato D, Santos J S, Escher G B, Ferreira B L, Maggio R M. Use of principal component analysis (PCA) and hierarchical cluster analysis (HCA) for multivariate association between bioactive compounds and functional properties in foods: A critical perspective. *Trends Food Sci Technol* **72**: 83–90 (2018)
- [58] Kim Y, Kim M, Lim J, Kim J T, Yoo C. Predictive monitoring and diagnosis of periodic air pollution in a subway station. *J Hazard Mater* **183**(1–3): 448–459 (2010)
- [59] Lee S, Liu H B, Kim M, Kim J T, Yoo C. Online monitoring and interpretation of periodic diurnal and seasonal variations of indoor air pollutants in a subway station using parallel factor analysis (PARAFAC). *Energy Build* **68**: 87–98 (2014)
- [60] Xia D, Vaye O, Yang Y N, Zhang H T, Sun Y F. Spatial distributions, source apportionment and ecological risks of C₉-C₁₇ chlorinated paraffins in mangrove sediments from Dongzhai Harbor, Hainan Island. *Environ Pollut* **270**: 116076 (2021)
- [61] Wold S, Sjöström M, Eriksson L. PLS-regression: A basic tool of chemometrics. *Chemom Intell Lab Syst* **58**(2): 109–130 (2001)



Hanwen WANG. He received his bachelor degree in Energy and Power Engineering in 2019 from Chang'an University in Xi'an, China. Then, he pursued his Ph.D. degree

at the Key Laboratory of Shaanxi Province for Development and Application of New Transportation Energy at the same university. His research interests include lubricant development and tribology.



Mingjin FAN. She received her Ph.D. degree in 2007 from the State Key Laboratory of Applied Organic Chemistry, Lanzhou University. In 2007, she went to Germany as a post doctor (Alexander von Humboldt Fellowship) and studied in the

Department of Chemistry in Technical University of Munich. On January 2009, she came back and began to work at the State Key Laboratory of Solid Lubrication, Lanzhou Institute of Chemical Physics, Chinese Academy of Sciences. From June 2014, she began to work in Baoji University of Arts and Sciences. Her research interests mainly focus on the investigation of new environmentally-friendly lubricants.



Rui DONG. She got her Ph.D. degree in 2021 from Lanzhou Institute of Chemical Physics (LICP) CAS, China. And now, she is doing postdoctoral work at Northwestern

Polytechnical University. From June 2021, she began to work at Baoji University of Arts and Sciences. Her research mainly focuses on the interfacial tribo-chemistry mechanism, design, synthesis, and tribological behavior of water-based lubricating materials.



Chunhua ZHANG. He received his Ph.D. degree from Chang'an University in 2002. His current position is professor and director of the Key Laboratory of Shaanxi

Province for Development and Application of New Transportation Energy. He is also the Chairman of Shaanxi Internal Combustion Engine Society. His research areas include lubrication of fuel and exhaust emissions of engines.